DETECTION OF DISPERSION CHARACTERISTICS OF APPARENT WAVE VELOCITY

Y. Fukumori (1)
M. Sako (1)
T. Kikuta (1)
K. Yanabu (1)
K. Toki (2)
Presenting Author; K. Yanabu

SUMMARY

Analyses were made of the dispersion properties of the apparent wave velocity detected from accelerograms for the frequency range 0.1 to 3Hz, which is most significant for the aseismic design of the buried pipe structures. An array observation system was built-up, and more than forty records of ground motion were obtained. Analyses were performed for longitudinal and transversal components with respect to the azimuthal direction. The calculated dispersion curves showed a strong dependence of the apparent wave velocity on the frequency component. Our results were used to establish an earthquake resistant design guideline for pipe structures.

INTRODUCTION

The apparent wave velocity is one of the most important factors used in the analysis of lifeline systems, especially those of buried pipe structures such as submerged tunnels and gas or water distribution systems. Deformation of buried pipe structures is governed by the relative motion of the surrounding ground at different arbitrary points on the axis of the pipe line. The ground motion of the surrounding soil is very similar to that of the free field because interaction between the soil and the pipe is not significant in the seismic response of pipes. The first approximation, therefore, of the strain induced in pipe is given by strain of the soil.

The axial strain ε is calculated from the following equation:

$$\varepsilon = |v/c|$$

in which, v is the particle velocity produced by the traveling wave along the pipe's axis and is the apparent wave velocity. v is easily determined from records of ground motion; whereas, c is determined neither from a record obtained at one observation site nor from records taken at sites that are not connected. Therefore a common time signal must be marked on all records in order to determine the wave velocity from seismograms obtained at different sites, this condition rarely obtains with ordinary strong motion accelerograph networks.

ARRAY OBSERVATION AND RECORDING SYSTEM

An array observation system was built-up in Yoshikawa township, 60km north of Tokyo. The observation area is close to the Edo river and ranges over an alluvial layer which thickens with the distance from the river

---

(1) Osaka Gas Co. Ltd., Japan.
(2) Professor, Disaster Prevention Research Inst., Kyoto Univ., Kyoto, Japan.

(Fig.1). The array consisted of four recording stations; one master station and three slave stations, in the shape of a triangle. The formation of the recording stations also is shown in Fig. 1; No.1 is the master station and Nos.2, 3 and 4 the slave stations. The solid and dashed lines represent the thickness of the alluvial deposit; i.e, the depth of the diluvial layer below the ground surface. The soil profiles at stations 1 and 3 are shown in Figs.3 and 4. The thickness of the alluvial deposit at these two stations differs markedly. This causes the depth of the diluvial layer to vary so sharply that these layers form a steep slope beneath the alluvial deposits. The shear and volumetric wave velocities of each layer were determined by the seismic prospecting.

Each recording station is equipped with two accelerographs, one at ground surface and one at the interface between the alluvial and diluvial layers. Schematic representations of the recording site and array formation are shown in Fig.2. The accelerograph is the three-component servo type and the recording device a digital cassette recorder with a frequency range of 0.1 to 30Hz and a dynamic range of 0.1 to 1000 gal. The slave stations are connected to the master station by public wire in order to receive a common time signal every two seconds. A buffer memory was prepared to obtain a three-second delay and the trigger level was set at 1gal.

Whenever the system is triggered, a signal is transmitted automatically by public wire to the monitoring room located in Osaka, about 500km apart from the site. The system has been operating for three years and has recorded more than 40 earthquakes. We analyzed 15 of these records. The epicenters of those 15 earthquakes are plotted in Fig.5.

FREQUENCY RESPONSE CHARACTERISTICS OF THE SITES

The recorded accelerograms were decomposed to obtain the longitudinal and transversal components with respect to the azimuthal direction for each earthquakes studied.

The frequency response functions were determined for the four stations from all the records studied and were defined as the ratio of the Fourier transform of the record at ground surface to that at the basal diluvial layer. But, because each frequency response function fluctuated, we performed a smoothing procedure in which several values for the frequency response functions were superposed for each recording station. The results in Fig. 6 give a comparison of the theoretical frequency response functions calculated by the multiple reflection theory from soil profiles at each recording station (Fig.7). This figure shows that the frequency response function is well determined by the multiple reflection theory and that the frequency response characteristics at each station are contained in each record. Moreover, it shows that the frequency characteristics at recording stations 1, 2 and 3 markedly differ.

Power spectral density functions were calculated from records obtained at the ground surface at each station and were superposed to diminish fluctuation. The results for the frequency response functions are given in Fig. 8. A comparison of this figure with Fig.7 shows that the frequency characteristics at each recording station are modified by the characteristics of the traveling path as well as those of the fault plane. Therefore, the predomi-

nant frequency at a recording station does not necessarily give the resonant frequency of the sites.

DETECTION OF APPARENT WAVE VELOCITY

Sum And Difference Method

The sum and difference method (Ref.1) was used to determine the apparent wave velocity from the records at the ground surface of two stations, the selection of which depended on the direction of wave transmission. Let $f_A(t)$ and $f_B(t)$ be the respective records at ground surface at stations A and B. Then the time lag between the two stations is a function of the frequency components and is calculated from the following relationship:

$$G(\omega, \tau) = \log\left\{\frac{H_-(\omega, \tau)}{H_+(\omega, \tau)}\right\}$$

$$H_+(\omega, \tau) = \left|\int_{-\infty}^{\infty}\{f_A(t+\tau) + f_B(t)\}e^{-i\omega t}dt\right|$$

$$H_-(\omega, \tau) = \left|\int_{-\infty}^{\infty}\{f_A(t+\tau) - f_B(t)\}e^{-i\omega t}dt\right|$$

in which, ω is the circular frequency and τ the time lag. When the phases of frequency components of the records at two stations coincide, the function $G(\omega, \tau)$ takes a large negative value, but this function takes a large positive value when out of phase by 180 degrees. The dependence of the time lag on the frequency component is shown in Fig.9. Once this sort of relationship is obtained, the time lag is easily converted to the apparent wave velocity and shows the dependence on the component frequency.

Using the method described above, we determined the dispersion characteristics of the apparent wave velocity for several pairs of records. Results are shown in Figs.10-12. In these figures, (L) and (T) stand for the longitudinal and transversal directions with respect to the azimuth, 2-S→3-S, for example, signifying that the records at our sites 2 and 3 were used to determine the relationship. Table 1 lists the earthquake data analyzed.

It is obvious that the apparent wave velocity depends greatly on the frequency component, even for such a low frequency range as 1.0Hz. Although the dispersion curves show much fluctuation, there is a geneal tendency that is similar for the longitudinal and transversal directions. The extent of the dependence of the apparent wave velocity on frequency, however, is different for each earthquake. This means that the dispersion characteristics are affected by the azimuthal direction, the epicentral distance, the depth of origin and so forth.

A comparison of the apparent wave velocities given in Figs.10-12 shows that an apparent wave velocity in a frequency range of less than 0.5Hz is small in sequence for earthquakes 18, 30 and 33 and that this sequence coincides with the sequence of the epicentral distance. Because the depth of the origin of these three earthqukes is almost same, the angle of incidence differs and the apparent wave velocity becomes rapid.

Phase Difference Method

Let $S_{xy}(\omega)$ be the cross power spectrum calculated from the records at stations X and Y and $R_{xy}(\tau)$ the auto-correlation function of the record at

station X. Then the cross spectrum $S_{xy}(\omega)$ is adjusted by the following equation to obtain the normalized cross spectrum $\rho_{xy}(\omega)$:

$$\rho_{xy}(\omega) = \frac{S_{xy}(\omega)}{R_{xx}(0)}$$

Earthquakes also were classified into several groups with respect to epicentral distance and azimuthal direction; these groups are given in Fig.5 as G1, G2, etc. The cross-correlation functions were stacked for all the records belonging to the same group in order to distinguish the correlation of frequency components between two stations after normalization by the standard deviations of respective records. An example of the cross-correlation function obtained by the phase difference method is shown in Fig. 13.

The Fourier transform of the cross-correlation function was calculated to obtain the phase spectrum. The coherence function $C_{xy}(\omega)$, also was calculated from the pair of cross-spectra by the following equation:

$$C_{xy}(\omega) = \frac{|\rho_{xy}(\omega)|^2}{S_{xx}(\omega)\, S_{yy}(\omega)}$$

in which $S_{yy}(\omega)$ is the power spectral density function of the record at station Y.

Examples of these functions are shown in Fig.14. Once the phase spectrum is obtained, in principle, the phase velocity is easily determined. But, in accelerograms in which a high frequency component is dominant, the phase angle fluctuates greatly (as in Fig.14); moreover, the correlation varies greatly for different frequencies. Therefore, a regression analysis was made by adopting the coherence function as a weighting function. The adopted regression curve $V(\omega)$ for the apparent velocity is

$$V(\omega) = \frac{a_2}{(a_0 + a_1 \omega^2)\sinh \omega} \qquad (a_0, a_1 \text{ and } a_2 \text{; constants})$$

Results are shown in Fig.15 for Groups 1, 3 and 4. The dispersion curve in this method is smooth compared with the curve obtained from the sum and difference method. It is, however, very difficult to determine the relationship for frequency components higher than 1.0Hz because the phase angles of high frequency components vary so sharply on the phase plane. The results shown in Fig.15 compare well with the relationship for a frequency range less than 1.0Hz.

Engineering Aspects

In terms of engineering, the lower bound of the wave velocity is important, and the lower envelope should be considered in the aseismic design of sructures in which the relative ground motion has a significant effect on the response. For a pipe line buried horizontally beneath the ground surface, the relative ground motion along the pipe's axis is the governing factor of the response of the pipe during an earthquake. The situation is very similar to the response of bridges with very long spans.

Based on the data given in Figs.10-12 and on the other records treated in this study, we adopted the tri-linear solid line shown in Figs.10-12 as the relationship between the apparent wave velocity against the frequency components in the tentative technical guideline for the earthquake resistant design of high pressure gas pipeline. This guideline was prepared by the Japan Gas Association according to the request of the Ministry of International Trade and Industry. In the guideline, the predominant period of the design ground motion is determined from the dynamic properties of the ground being investigated to determine the apparent wave velocity which then can be converted into the wave length when necessary. Moreover, the particle velocity of the ground is given by the response spectrum provided in the same guideline. Then, once the wave length has been determined, the strain induced in the ground is calculated, and this is converted into the strain on the pipe by the prescribed procedures (Ref.2).

CONCLUSIONS

An array observation system was built-up to obtain records of the ground motion for the frequency range that affects the seismic behavior of buried pipe lines such as gas and water supplies. To determine the dependence of the apparent wave velocity on the frequency components, we analyzed the recorded accelerograms by two methods and concluded.

(1) It is possible to determine the dispersion characteristics for the frequency range which affects on the structural response of a buried pipe line.

(2) The apparent wave velocity depends mainly on the frequency components, and it decreases at increasing frequencies higher than 1.0Hz.

(3) The apparent wave velocity for a frequency range higher than 0.3seconds is close to the shear wave velocity of the ground when the epicentral distance is great and the depth of the earthquake's origin is shallow compared to this distance.

(4) Dispersion characteristics vary. They depend on the such properties of earthquakes as the epicentral distance, the depth of the origin, the azimuthal direction, etc.

(5) The lower bound of the apparent wave velocity for a frequency lower than 1.0Hz is 1.0km/sec.

REFERENCES

1. Dziewonski, A.M. and A.L. Hales : Numerical Amalysis of Dispersed Seismic Waves, Methods in Computational Physics, Vol.II, Academic Press, 1972, pp.39-85.

2. Toki, K. Fukumori, Y. Sako, M. and Tsubakimoto, T. : Recommended Practice for Earthquake Design of High Pressure Gas Pipelines, Proc. of 1983 International Symposium on Lifeline Earthquake Engineering, The 4th National Congress on Pressure Vessel and Piping Technology, ASME, 1983, pp.349-356.

Table 1 Observed Earthquakes

No.	Date	Epicenter N	Epicenter E	Depth	Epicentral Distance	Magnitude	During time	Maximum Acceleration	Group
				km	km		sec		
5	'81.11.9	35.6°	140.2°	40	43	4.1	17	5.2	
15	'81.1.9	38.6	140.3	0	411	7.0	58	6.4	
21	'81.2.22	36.5	140.7	50	101	4.7	20	4.7	3
23	'81.3.6	32.2	138.3	360	436	5.5	22	3.5	5
24	'81.3.12	35.9	140.3	60	36	4.7	23	13.0	
30	'81.9.14	36.2	140.0	70	25	4.8	14	10.4	4
31	'81.11.30	36.1	139.9	50	23	4.4	19	11.0	4
33	'82.3.7	36.5	140.7	60	94	5.6	29	19.0	3
41	'82.4.19	36.1	139.9	50	23	4.9	28	7.6	4
49	'82.7.23	36.2	142.0	30	189	7.0	252	31.6	1
53	'82.7.25	36.3	141.8	10	178	5.9	83	3.4	1
57	'82.8.14	36.4	141.2	40	131	5.6	51	4.6	2
58	'82.8.16	36.5	141.0	40	121	5.5	34	3.0	2
60	'82.8.24	36.4	141.5	30	152	5.8	69	5.4	2
63	'82.9.6	29.5	141.0	190	717	6.9	40	5.8	5

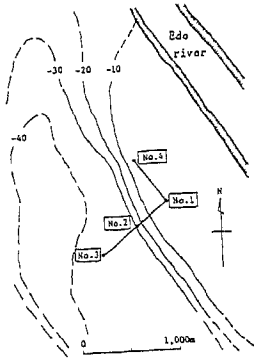

Fig.1 Disposition of Observation Stations and Depth of Diluvial Layer

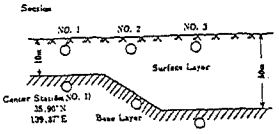

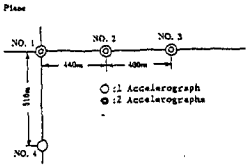

Fig.2 Location of Accelerographs

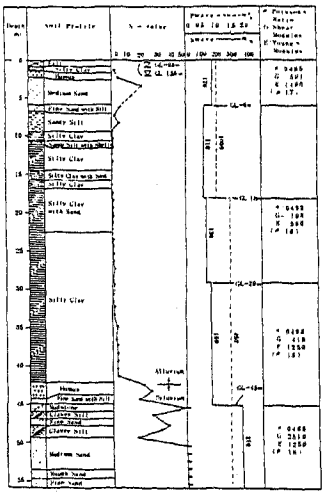

Fig.4 Soil Profile (Point No.3)

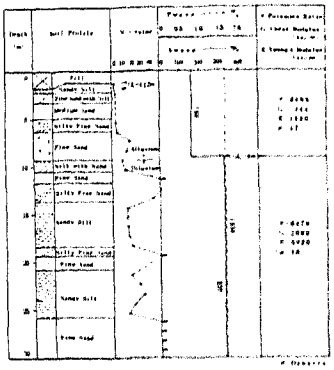

Fig.3 Soil Profile (Point No.1)

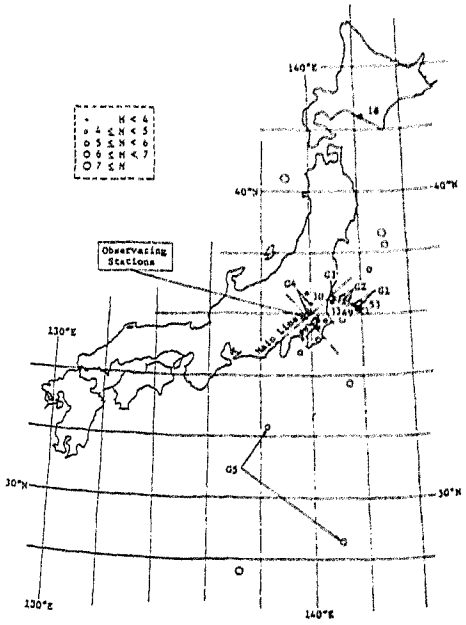

Fig.5 Epicenter and Magnitude

	Model of the Ground			
	h(%)	Vs(m/s)	ρ(g/cm³)	H(m)
Point 1	2.5	160	1.8	9
	2.5	330	1.9	∞
	h(%)	Vs(m/s)	ρ(g/cm³)	H(m)
Point 2	2.5	130	1.8	9
	2.5	170	1.8	5
	2.5	120	1.5	5
	2.5	330	1.9	∞
	h(%)	Vs(m/s)	ρ(g/cm³)	H(m)
Point 3	2.5	170	1.8	6
	2.5	110	1.5	12
	2.5	130	1.55	11
	2.5	160	1.6	16
	2.5	370	2.0	∞
	h(%)	Vs(m/s)	ρ(g/cm³)	H(m)
Point 4	2.5	100	1.8	6
	2.5	170	1.8	3
	2.5	380	1.9	∞

Fig.6 Soil Profile Models

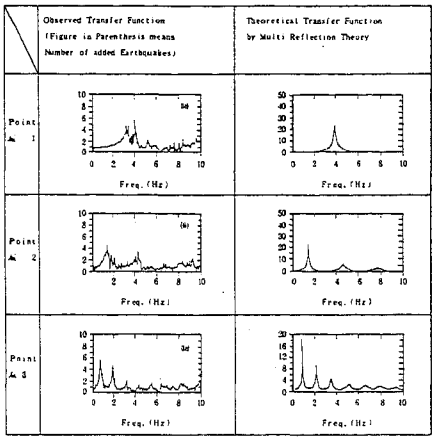

Fig.7 Observed and Theoretical Transfer Function

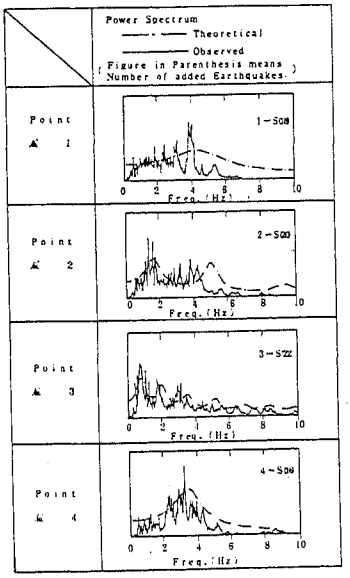

Fig.8 Power Spectrum

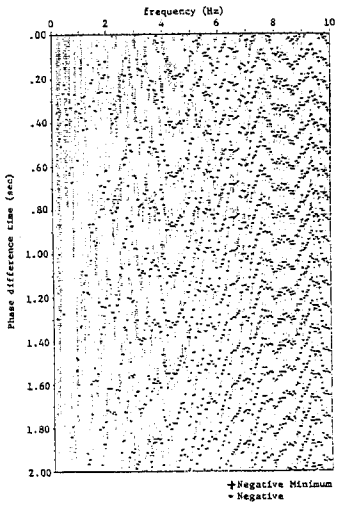

Fig.9 G(w, T) chart
(Earthquake No.30 TR Component)

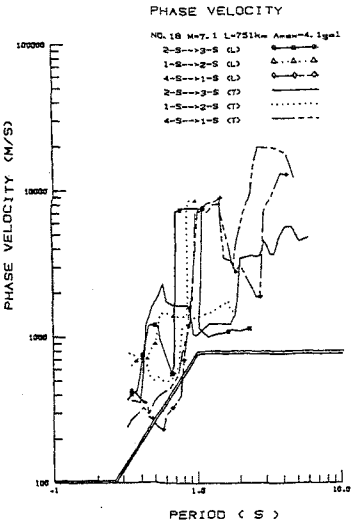

Fig.10 Phase Velocity
(Earthquake No.18)

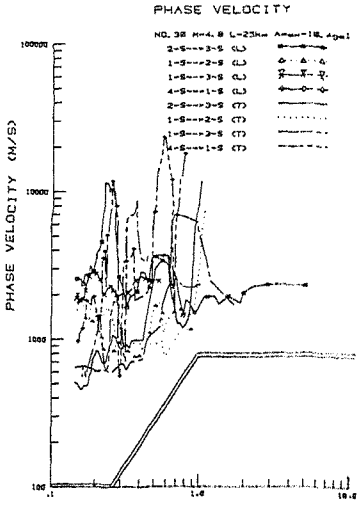

Fig.11 Phase Velocity
(Earthquake No.30)

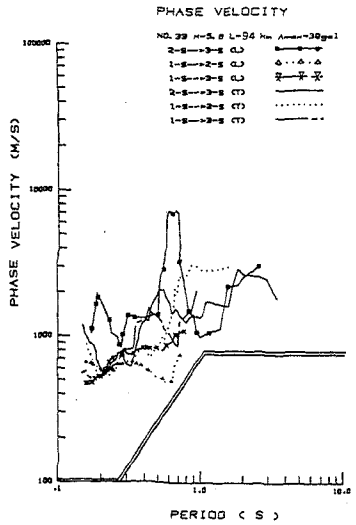

Fig.12 Phase Velocity
(Earthquake No.33)

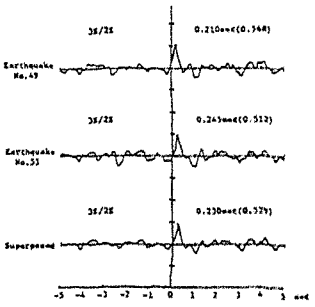

Fig.13 Cross-Correlation

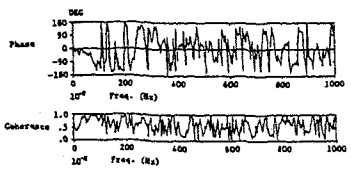

Fig.14 Phase Spectrum and
Coherence Function

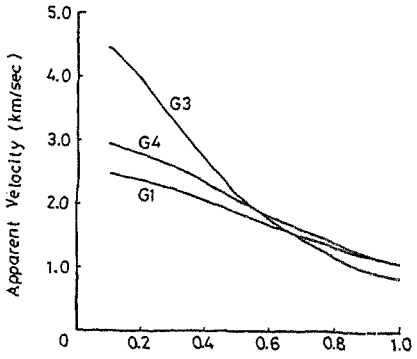

Fig.15 Apparent Wave Velocity
by Regression Analysis